Journal of Power Sources 199 (2012) 263–269

Contents lists available at SciVerse ScienceDirect

Journal of Power Sources

journal homepage: www.elsevier.com/locate/jpowsour

A new cathode material $Na_2V_6O_{16}\cdot xH_2O$ nanowire for lithium ion battery

Haiyan Wang[a,*], Wenjie Wang[a], Yu Ren[b], Kelong Huang[a,*], Suqin Liu[a]

[a] School of Chemistry and Chemical Engineering, Central South University, Changsha, Hunan 410083, PR China
[b] EaStChem and School of Chemistry, University of St Andrews, St Andrews, Fife KY16 9ST, UK

ARTICLE INFO

Article history:
Received 10 May 2011
Received in revised form 30 August 2011
Accepted 12 October 2011
Available online 24 October 2011

Keywords:
Li-ion battery
Cathode
Sodium hexavanadate nanowire
Hydrothermal method
Thermal treatment
Electrochemical performance

ABSTRACT

Single crystalline $Na_2V_6O_{16}\cdot 2.36H_2O$ nanowires are synthesized by a facile hydrothermal method as a new cathode material for Li-ion battery. The nanowires show a diameter of 60–100 nm and a length of up to 5 μm. Appropriate thermal treatment could effectively improve the cycling performance, although the discharge capacity is sacrificed to some extent. $Na_2V_6O_{16}\cdot 0.86H_2O$ after heat treatment under 300 °C delivers an initial specific discharge capacity of 235.2 mAh g^{-1} at 30 mA g^{-1}, with a capacity retention of 91.1% after 30 cycles. Long cycling test is demonstrated by the retention of 90.4% and 94.4% at 150 and 300 mA g^{-1}, respectively, after 80 cycles. Good rate capability is also achieved for this material. It is proposed that the improved cycling stability of the electrode after thermal treatment is mainly attributed to the removal of a part of crystal water, accompanied with certain structural arrangement.

1. Introduction

The commercial Li-ion battery mainly involves the use of a layered structure transitional metal oxide, e.g. $LiCoO_2$ as positive electrode material [1]. Unfortunately, $LiCoO_2$ only enables to deliver a reversible capacity of about 140 mAh g^{-1} typically charged to 4.2 V. In addition, it is still associated with some other disadvantages, such as high cost, toxity and poor overcharge property [1–3]. For above reasons, $LiCoO_2$ is hard to meet the requirement of next generation rechargeable batteries for electrical vehicle [3]. Accordingly, considerable efforts have been successively made to propose new positive electrode materials with higher capacity for Li-ion battery [4–8].

There has been increased interest in synthesizing the nanostructural vanadium oxides and their derivative compounds as cathode materials due to their outstanding structure flexibility, high discharge capacity, and low cost [8–13]. Of these the most studied is lithium trivanadate ($Li_{1+x}V_3O_8$) [11,12]. However, to the best of our knowledge, LiV_3O_8 could not be obtained by one-step hydrothermal method. In our previous work, a new cathode material ammonium trivanadate with a maximum discharge capacity of 225.9 mAh g^{-1} and good cycling stability was reported by one-step hydrothermal reaction [14]. It was found that both Li^+ in LiV_3O_8 and NH_4^+ group in $NH_4V_3O_8$ could not be extracted from the host materials and probably acted as pillar to stabilize the crystal structure [11,14]. Actually, in $Li_xV_3O_8$, there are two kinds of storage sites for lithium ions (octahedral and tetrahedral sites). Almost Li ions in LiV_3O_8 are accommodated at the octahedral sites in the interlayer, which are immobile, only those at the tetrahedral sites between the layers can take part in insertion/deinsertion processes. Information above inspires us to use other cations, such as Na^+ or K^+ to replace Li^+ or NH_4^+ to form new cathode materials for Li-ion battery.

Sodium vanadate compounds have been found to be potential Li^+ intercalated electrode materials [8,10,15–17]. Kawakita et al. [16] investigated the effect of crystallinity on the lithium insertion behaviour of $Na_{1+x}V_3O_8$. $Li_3NaV_3O_8$ was synthesized via aqueous precipitation and subsequently chemically lithiation by Spahr et al. [17]. It had a reversible specific capacity of 215 mAh g^{-1} between 1.5 and 4.0 V with good cycling performance [17]. Liu et al. [10] fabricated NaV_6O_{15} nanorods by hydrothermal method, delivering a high discharge capacity of 328 mAh g^{-1}. There are several reports about $Na_2V_6O_{16}\cdot xH_2O$ [18–20]. Zhou et al. [18] reported the hydrothermal synthesis of $Na_2V_6O_{16}\cdot 3H_2O$ nanowires based on the reaction of V_2O_5 and Na_2SO_4 with the initial pH of 5.5. Yu et al. [19] successfully synthesized the $Na_2V_6O_{16}\cdot 3H_2O$ nanobelt using V_2O_5 and NaF as raw materials and they found that the presence of F ion was crucial for the formation of the material with such morphology. $Na_2V_6O_{16}\cdot nH_2O$ nanowires are fabricated by a low-temperature hydrothermal route using V_2O_5, H_2O_2 and NaOH, without the addition of any organic surfactant or inorganic ions [20]. However, there are no records on its electrochemical performance, especially as a cathode material for Li-ion battery. It should be noted that $Na_2V_6O_{16}\cdot 3H_2O$ shows different crystal structure from

* Corresponding authors. Tel.: +86 731 88879850; fax: +86 731 88879850.
E-mail addresses: wanghy419@126.com (H. Wang), klhuang@mail.csu.edu.cn (K. Huang).

0378-7753/$ – see front matter © 2011 Elsevier B.V. All rights reserved.
doi:10.1016/j.jpowsour.2011.10.045

NaV_3O_8 [16,17], which probably means different electrochemical properties. In current work, we first propose a new cathode material, sodium hexavanadate nanowire ($Na_2V_6O_{16}\cdot 2.36H_2O$) for Li-ion battery by a new and facile preparation method, which gives an initial specific discharge capacity of 268 mAh g^{-1}. After appropriate thermal treatment, the nanowire exhibits much better cycling stability.

2. Experimental

2.1. Synthesis and characterization of $Na_2V_6O_{16}\cdot xH_2O$

The starting materials, V_2O_5 and sodium hydroxide were of analytically pure grade. Firstly, 1.819 g V_2O_5 and 0.400 g NaOH were dissolved in deionized water successively. The mixed solution was then transferred to 50 ml Teflon lined stainless steel autoclave. The total volume of the solution was about 40 ml. The autoclave was sealed and heated at 180 °C for 48 h and then cooled to room temperature naturally. The obtained precipitates were filtered, washed with deionized water three times. Finally, the precipitates were dried at 80 °C overnight to obtain the $Na_2V_6O_{16}\cdot 2.36H_2O$ powder. For comparison, some parts of product were further heated 2 h at 300 °C and 400 °C in air, respectively.

All X-ray diffraction (XRD) data were given by a Philips X-Pert system (Cu-Kα radiation) with a step of 0.02°. Fourier transform infrared (FT-IR) spectra were recorded using the Nicolet 6700 FT-IR spectrometer. Thermal gravimetry (TG) was carried out with a NETZSCH STA 449C differential scanning calorimeter under N_2 atmosphere at a ramping rate of 10 °C min^{-1}. Morphological studies were conducted using a JSM6430F scanning electron microscopy (SEM) and a JEOL JEM-2011 transmission electron microscopy (TEM) employing a LaB6 filament as the electron source and an accelerating voltage of 200 keV.

2.2. Electrochemical measurements

The electrochemical cells were constructed by mixing the active material, polyvinylidene fluoride (PVDF), and Super S carbon in the weight ratio of 80:10:10. Tetrahydrofuran was used as solvent. The slurry was cast onto Al foil. After drying well, the electrodes were assembled into CR2016 coin-type cells with commercial electrolyte (Merck; 1 M $LiPF_6$ in 1:1, v/v, ethylene carbonate/dimethyl carbonate) and a Li metal as counter electrode. The cells were constructed in an Ar-filled MBraun glovebox and cycled galvanostatically between 1.5 and 4.0 V (voltage unit in this paper is versus Li/Li^+) at a desired current density with a Land CT2001A tester system at room temperature. Cyclic voltammetry (CV) was operated using electrochemical station (Shanghai Chenhua, China) with scan rate 0.1 mV s^{-1} between 1.5 and 4.0 V at room temperature. Electrochemical impedance spectroscopy (EIS) was recorded by the Solartron analytical instrument over the frequency range from 500 kHz to 10 mHz with an amplitude of 5 mV. Before testing, each cell was charged to 2.5 V and then kept at that voltage for 8 h.

3. Results and discussion

Fig. 1 shows XRD patterns of the as-prepared products with and without thermal treatment. All the diffraction lines in XRD pattern a can be readily indexed to a monoclinic crystalline $Na_2V_6O_{16}\cdot 3H_2O$ phase (space group $P2_1/m$) with the lattice parameters $a = 1.1616$ nm, $b = 0.3630$ nm, $c = 0.7789$ nm and $\beta = 93.91°$, as shown in Table 1, which are a little different from those of standard $Na_2V_6O_{16}\cdot 3H_2O$ (JCPDS No. 16-0601) and the literature values [19]. The difference of lattice parameters should be ascribed to different contents of crystal water in formula, proved by the following TG results. Meanwhile, no other diffraction line is found, indicating the as-prepared $Na_2V_6O_{16}\cdot xH_2O$ is pure phase. For patterns b and c, they still keep the monoclinic structure well after thermal treatment, although the strongest diffraction peak (0 0 1) shifts toward positive angle and diffraction peaks of (−3 0 1), (1 1 1) and (−2 1 1) move to negative direction, in comparison with the pristine material. In addition, the intensity of some diffraction peaks reduces. The lattice parameters of material treated at 300 °C are indexed as follows: $a = 1.0884$ nm, $b = 0.3641$ nm, $c = 0.7032$ nm and $\beta = 88.62°$. Clearly, as seen from Table 1, the annealed materials indicate much smaller unit cell volume (0.2796 nm^3 at 300 °C, 0.2527 nm^3 at 400 °C) than that (0.3276 nm^3) of material without thermal treatment, suggesting certain structural arrangement appears with contracting a axis, as well as decreasing β value. This is probably due to the removal of some crystal H_2O during the thermal treatment, which is further verified by the FT-IR results in Fig. 2 and TG curves in Fig. 3. The dehydration of nanowires could be described as well-known topotactic dehydration [21].

Table 1
The roughly calculated lattice parameters of $Na_2V_6O_{16}\cdot xH_2O$: (a) without thermal treatment; (b) with thermal treatment at 300 °C for 2 h; and (c) with thermal treatment at 400 °C for 2 h.

Samples	a (nm)	b (nm)	c (nm)	β (°)	V (nm^3)
a	1.1616	0.3630	0.7788	93.906	0.3276
b	1.0884	0.3641	0.7032	88.619	0.2786
c	0.9642	0.3705	0.7076	88.602	0.2527

As observed, all three samples have similar absorption bands at about 3462.8, 1635.1, 997.8, 958.0, 737.7 and 550.4 cm^{-1}, respectively. Apparently, the bands at 997.8 and 958.0 cm^{-1} are due to V=O stretching of distorted octahedral and distorted squarepyramids, while those at 737.7 and 550.4 cm^{-1} are assigned to asymmetric and symmetric stretching vibration of V–O–V bonds, respectively [22]. In addition, there are two another bands at 3462.8 and 1635.1 cm^{-1}, corresponding to crystal H_2O in the $Na_2V_6O_{16}\cdot xH_2O$ formula [23]. It should be noted that the bands of sample b and c due to crystal H_2O in Fig. 1b are much weaker than that of sample a, implying some crystal H_2O were removed after thermal treatment. Comparatively, more crystal H_2O should be removed with high thermal treatment based on the intensity of band at about 1635.1 cm^{-1}. Furthermore, the right enlarged view clearly indicates the shift of the band at 737.7 cm^{-1} toward the

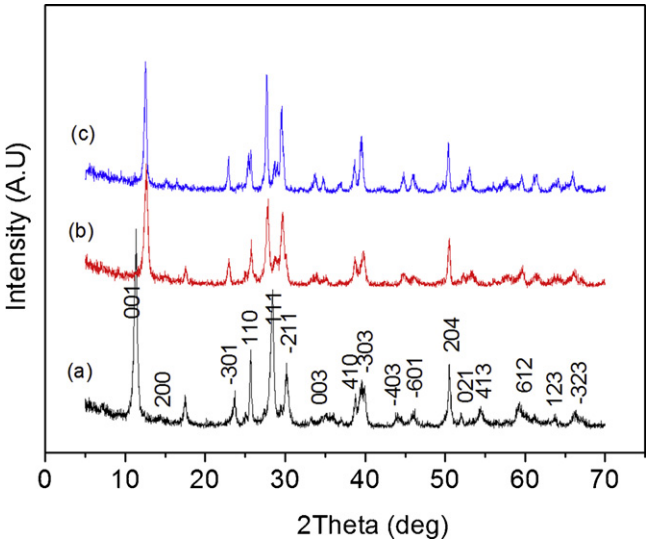

Fig. 1. XRD patterns of the as-prepared $Na_2V_6O_{16}\cdot xH_2O$ powder: (a) without thermal treatment; (b) with thermal treatment at 300 °C for 2 h; and (c) with thermal treatment at 400 °C for 2 h.

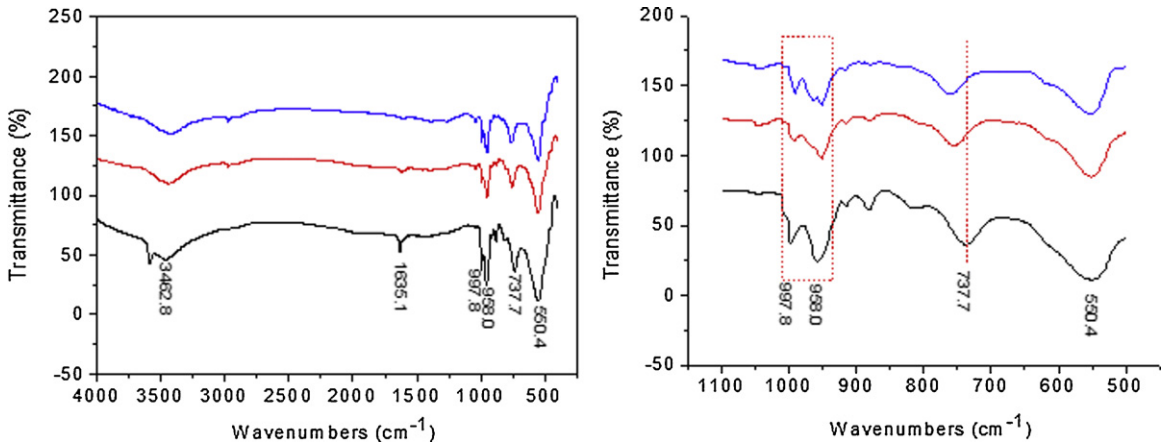

Fig. 2. FT-IR spectra of the as-prepared $Na_2V_6O_{16}{\cdot}xH_2O$ powder: (a) without thermal treatment; (b) with thermal treatment at 300 °C for 2 h; and (c) with thermal treatment at 400 °C for 2 h.

high frequency and the complication of bands between 997.8 and 958.0 cm^{-1}, which further confirm the slight structural arrangement due to the loss of crystal water. TG tests of $Na_2V_6O_{16}{\cdot}xH_2O$ without thermal treatment and with thermal treatment at 300 °C were chosen to verify the amount of crystal water. TG curves in Fig. 3 reveal a 6.53% mass loss for sample a from 100 to 400 °C and a 2.50% mass loss for sample b [19]. It is thereby deduced that the amount of crystal water in sample a and b is about 2.36 and 0.86 per unit, respectively. Thus, results of XRD, FT-IR and TG studies leave no doubt that the as-prepared material without thermal treatment is $Na_2V_6O_{16}{\cdot}2.36H_2O$, while that with thermal treatment at 300 °C is composed of $Na_2V_6O_{16}{\cdot}0.86H_2O$. For simplicity, the products are sometimes written as $Na_2V_6O_{16}{\cdot}xH_2O$ unless stated otherwise. In our previous work [14], it is found that crystal water in $NH_4V_3O_8$ compound usually affected its structure, probably further its electrochemical performance.

The morphology of $Na_2V_6O_{16}{\cdot}2.36H_2O$ is shown in Fig. 4. As observed, the as-prepared material is of nanowire shape with 60–100 nm in diameter and up to 5 μm in length. From Fig. 4b and c, it is noted that some of primary nanowires are partially attached together to form bundles. Actually, some of bundles have large diameter, even up to several micrometers. A more close observation on individuals is depicted by the high-resolution TEM images (Fig. 4d). Note that the as-prepared material is beam-sensitive under a high accelerated voltage of 200 kV. Thus, it is hard to obtain perfect HRTEM image. But from the un-destroyed parts, it could be seen that the nanowire is structurally uniform, free from dislocations and defects. Meanwhile, the lattice fringe parallel to the longitudinal direction with an inter-planar distance of 0.72 nm can be clearly observed, which matches well with the d-spacing of (0 0 1) planes of monoclinic layered $Na_2V_6O_{16}{\cdot}2.36H_2O$ in Fig. 1. HRTEM result also demonstrates the single crystalline nature of the nanowire. Note that nano-scaled materials can generally provide a high specific surface area and short ion diffuse pathway, compared with that of bulk material, both of which are beneficial to the electrochemical performance [24–26]. Undoubtedly, $Na_2V_6O_{16}{\cdot}xH_2O$ nanowire in this work would provide better electrochemical properties than that with normal morphology since the intercalation and de-intercalation of Li^+ between the layers of cathode is a diffusion process [13,14]. Fig. 5 shows the morphology of annealed sample at 300 °C, indicating that thermal treatment could break some of long wires and increase the diameter of wire bundles.

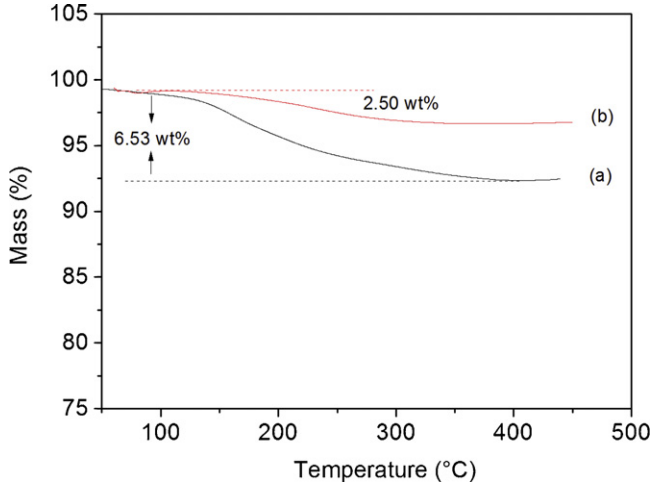

Fig. 3. TG curves of the as-prepared $Na_2V_6O_{16}{\cdot}xH_2O$ powder: (a) without thermal treatment and (b) with thermal treatment at 300 °C for 2 h.

The CV comparison (Fig. 6) results indicate the electrochemical difference of the as-prepared three $Na_2V_6O_{16}{\cdot}xH_2O$. There are two main redox peaks in Fig. 6a with overlapping oxidation peaks at about 2.68 V and corresponding reduction peaks at 2.43, 2.60 V, respectively. A very slight pair of redox peak at 3.72 V is also observed. For the annealed samples, the pair of redox peaks at about 3.7 V is more obvious and a new reduction peak at 3.14 V appears, of which the intensity increases with the increasing of the annealed temperature. Moreover, the oxidation peaks in the initial oxidation curve between 2.4 and 2.8 V of the annealed samples split well. However, the overlapping oxidation peaks are also shown in subsequent cycles. It is well known that the redox peaks correspond to the lithium ion insertion and extraction processes during the cycling. Clearly, the annealed samples show more complicated Li intercalation/deintercalation behaviour. The splitting of many redox peaks was ascribed to the different lithium sites with energy difference for lithium ions holding [27]. The CV results further confirm the slight structural arrangement of the annealed samples.

Electrochemical performance of $Na_2V_6O_{16}{\cdot}xH_2O$ electrodes at a current density of 30 mA g^{-1} between 1.5 and 4.0 V is compared in Fig. 7A. Fig. 7B shows the third corresponding load curves. $Na_2V_6O_{16}{\cdot}2.36H_2O$ electrode delivers a high initial specific discharge capacity of 268.0 mAh g^{-1} (about 6.5 electrons per unit formula are exchanged) and the discharge capacity retains 201.4 mAh g^{-1} at the 30th cycle (75.2% of the initial capacity). It is considered that Na^+ in $Na_2V_6O_{16}{\cdot}2.36H_2O$ is situated at octahedral sites between the layers composed of vanadium and oxygen atoms. The vacant tetrahedral sites are available for occupation of Li ions [17,28]. In the case of $Na_2V_6O_{16}{\cdot}0.86H_2O$ after thermal treatment

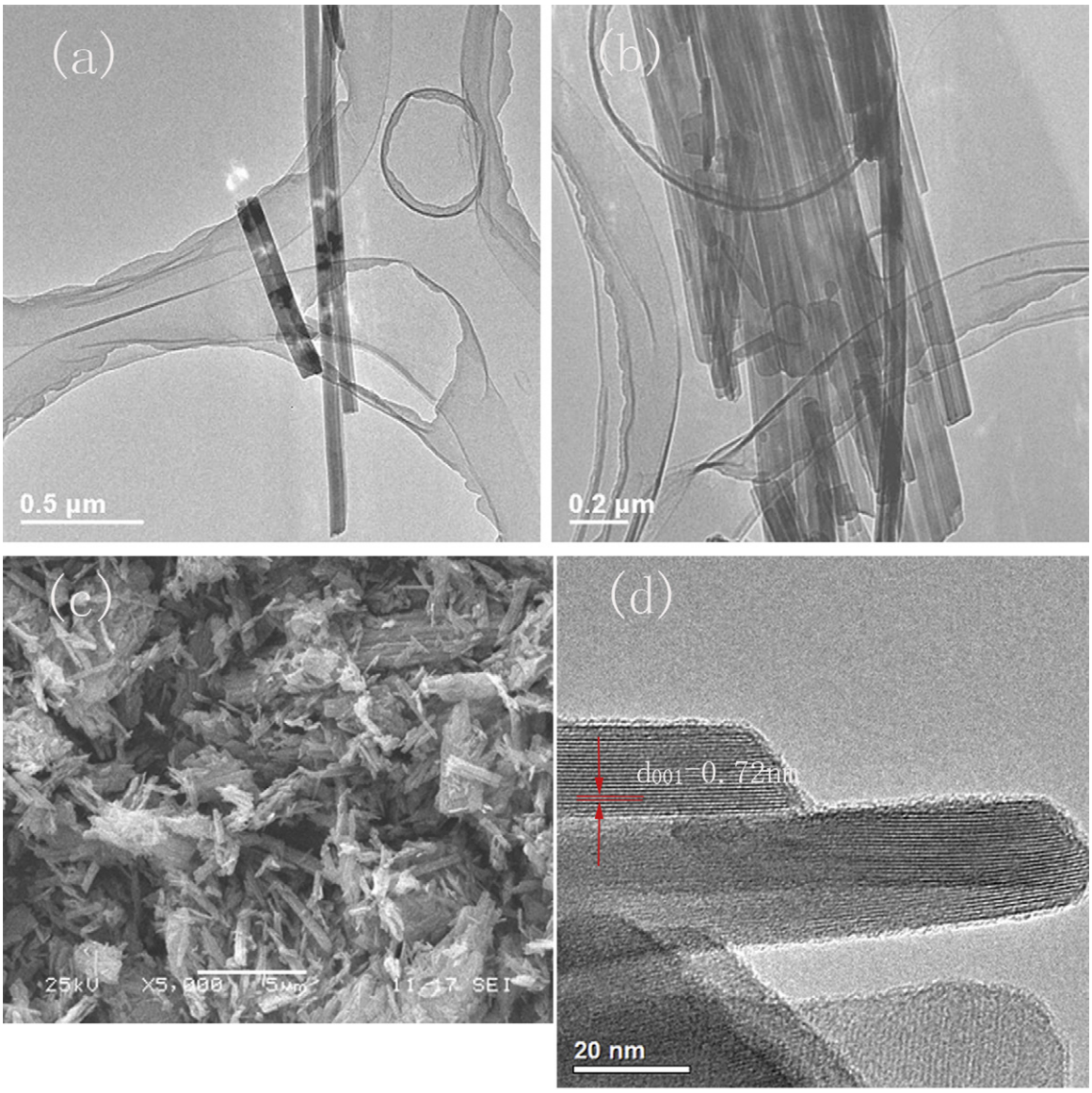

Fig. 4. TEM (a and b), SEM (c) and high-resolution TEM (d) images of $Na_2V_6O_{16}\cdot 2.36H_2O$ powder.

at 300 °C, it exhibits improved cycling stability with capacity retention of 91.1% after 30 cycles, although the initial discharge capacity decreases to 235.2 mAh g^{-1}. When heated at 400 °C, the initial discharge capacity of the sample further decreases to 189.2 mAh g^{-1}. It increases gradually to 200 mAh g^{-1} at the fifth cycle then keeps quite stable with the capacity retention of 99% after 30 cycles. Apparently, the sample without heat treatment possesses poor cycling stability, while the annealed samples show much better

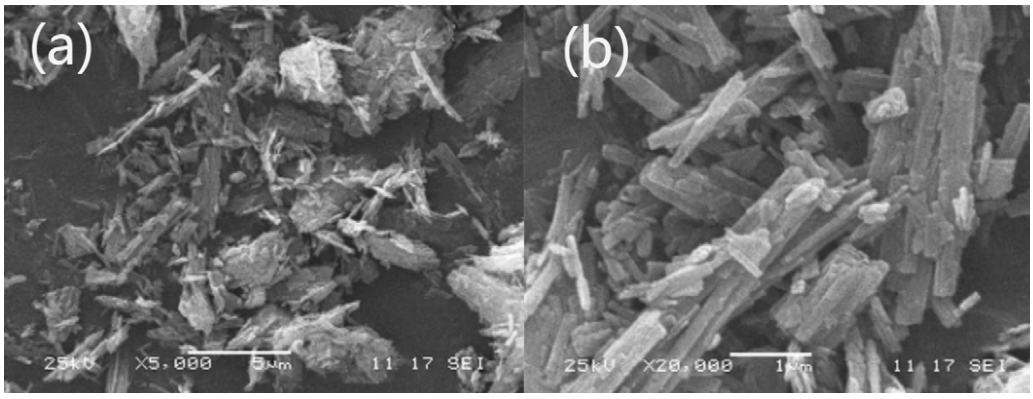

Fig. 5. SEM images of the as-prepared $Na_2V_6O_{16}\cdot 0.86H_2O$.

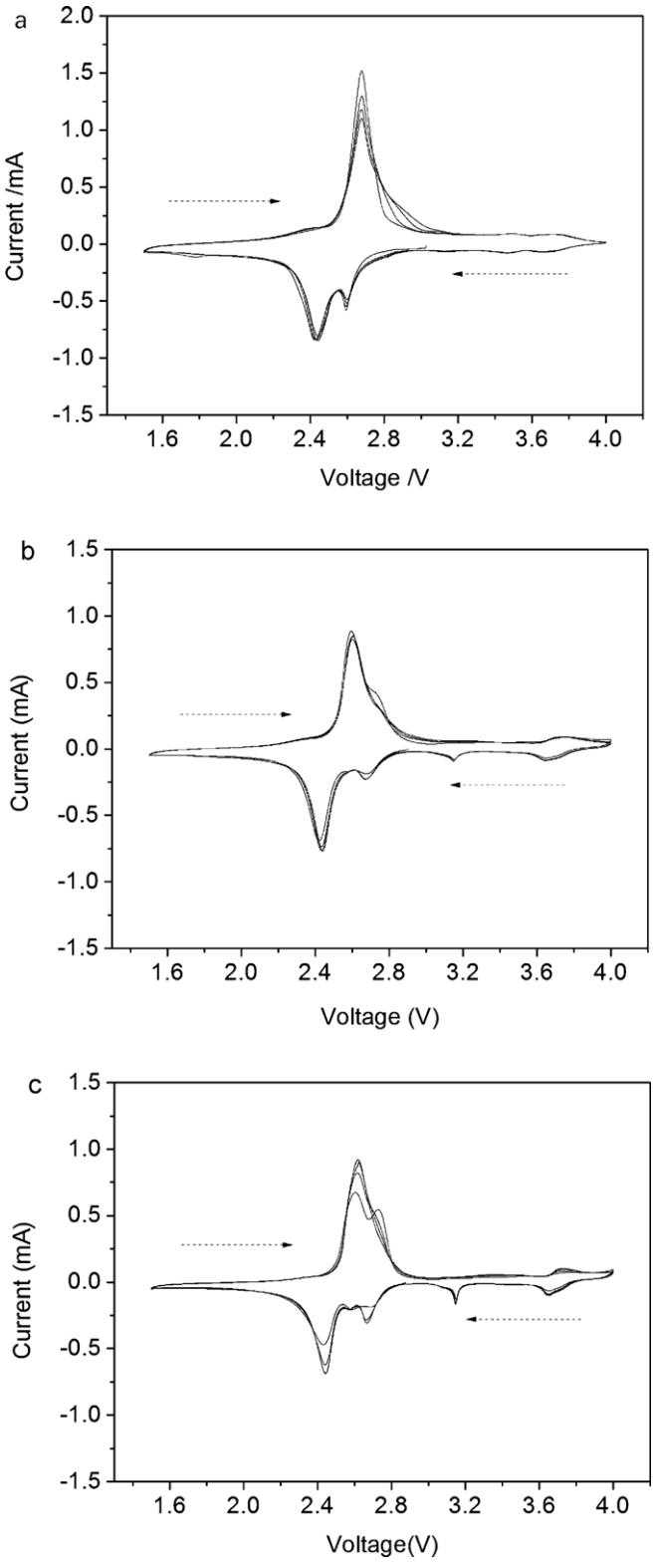

Fig. 6. Cyclic voltammetry curves of the as-prepared $Na_2V_6O_{16}{\cdot}xH_2O$ powder: (a) without thermal treatment; (b) with thermal treatment at 300 °C for 2 h; and (c) with thermal treatment at 400 °C for 2 h, operating between 1.8 and 4.0 V at scanning rate 0.1 mV s^{-1}.

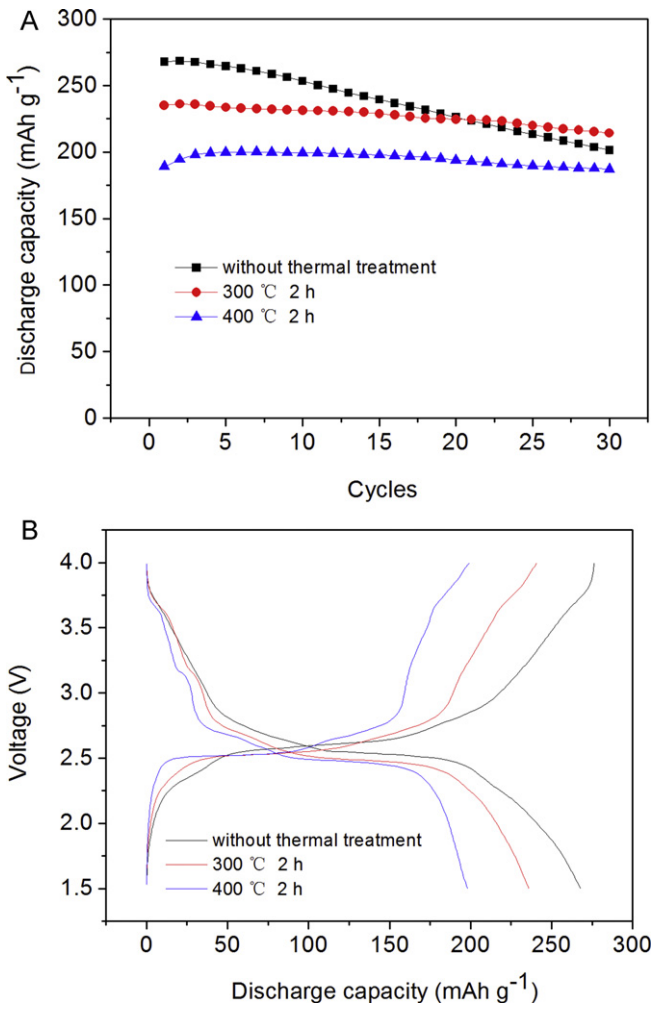

Fig. 7. (A) Cycling performance and (B) the third load curves of the as-prepared $Na_2V_6O_{16}{\cdot}xH_2O$ powder: (a) without thermal treatment; (b) with thermal treatment at 300 °C for 2 h; (c) with thermal treatment at 400 °C for 2 h, at 30 mA g^{-1} between 1.8 and 4.0 V.

cycling stability. Furthermore, the capacity retention is increased with the enhanced heating temperature. It is worthwhile to note that high heating temperature sacrifices the discharge capacity, probably due to increased activation energy of migrated lithium ions and the less available sites for lithium ions in shrunk crystal. The detailed explanation is proposed as follows: generally, the structure of $Na_2V_6O_{16}{\cdot}xH_2O$ can be described as $V_3O_8^-$ puckered layers held together by Na^+, which almost occupies the octahedral sites in each crystallite. The crystal water is located between the layers and the migrated lithium ions after discharge process are accommodated at the tetrahedral sites. As shown in Fig. 1 and Table 1, the annealed samples had much smaller parameters and shrunk crystal volume, which would result in the change of interlayer distance and further contraction of the lithium ion diffusion path. That is, the activation energy of migration of lithium ions would increase after annealing, while the available sites for lithium ions would decrease slightly. Therefore, at the same current density, less lithium ions could be inserted into the host material. It is well known that vanadate compounds usually suffer from large capacity fading due to their poor structural stability [8,17]. The reduced capacity and improved cycling performance of annealed samples should be ascribed to the loss of crystal water, accompanied with the structural arrangement. That is to say, crystal water in $Na_2V_6O_{16}{\cdot}xH_2O$ could play a negative role in stabilizing the structure during Li^+ insertion and extraction [29]. Actually, the annealed

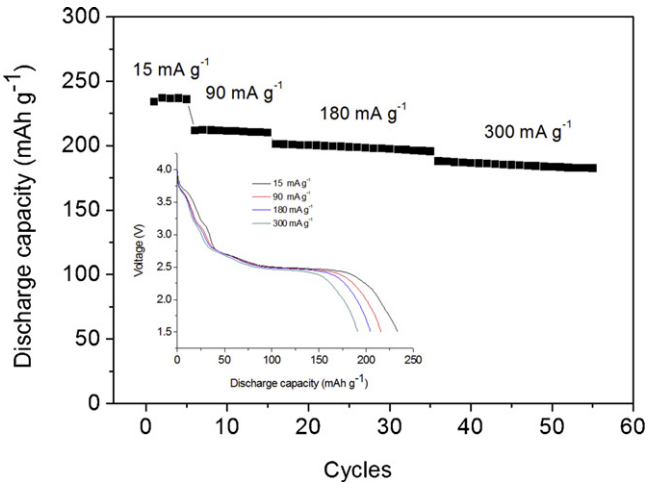

Fig. 8. Rate capability of the as-prepared $Na_2V_6O_{16}{\cdot}0.86H_2O$ electrode, together with the initial discharge curves at various rates inset.

samples indicate much smaller lattice parameters coupled with lattice volume (Table 1), which would be more stable when upon long cycling [30,31]. Liu et al. found [10] that appropriate heat treatment could improve the crystallization of NaV_6O_{15}, which was beneficial for the electrochemical performance.

The rate performance at up to 300 mA g^{-1} of the $Na_2V_6O_{16}{\cdot}0.86H_2O$ is investigated (Fig. 8). The inset is the initial discharge capacity curve at various current densities, indicating good charge–discharge plateau. As can be seen, $Na_2V_6O_{16}{\cdot}0.86H_2O$ delivers the discharge capacity of 236.9, 212.0, 201.1, and 188.1 mAh g^{-1} at 15, 90, 180, 300 mA g^{-1}, respectively. The discharge capacity decreases a little with the increasing of charge–discharge current density, unlike the $(NH_4)_{0.5}V_2O_5$ in our recent work [32]. Surprisingly, no obvious capacity fading is observed. Above results demonstrate that $Na_2V_6O_{16}{\cdot}0.86H_2O$ shows good rate capability.

Fig. 9a depicts the long cycling performance of $Na_2V_6O_{16}{\cdot}0.86H_2O$ electrode between 1.5 and 4.0 V at 150 and 300 mA g^{-1}. The discharge curves at different cycles at 150 mA g^{-1} is also attached. The initial discharge capacity of the $Na_2V_6O_{16}{\cdot}0.86H_2O$ at 150 and 300 mA g^{-1} is 200.6 and 189.0 mAh g^{-1}, respectively. Both cells were firstly tested for 1 cycle at 30 mA g^{-1} for activation. Excellent cycling stability with the capacity retention of 90.4% at 150 mA g^{-1}, 94.4% at 300 mA g^{-1} is achieved after 80 cycles. Meantime, good plateau retention ability for $Na_2V_6O_{16}{\cdot}0.86H_2O$ is obviously observed in inset load curves (Fig. 9a). For $Na_2V_6O_{16}{\cdot}xH_2O$ treated at 400 °C, no capacity fading is found at a current density of 300 mA g^{-1} even after 100 cycles, as shown in Fig. 9b. It maintains the discharge capacity of 170.0 mAh g^{-1} at the 100th cycle. Results above further confirm the excellent cycling performance of the annealed $Na_2V_6O_{16}{\cdot}xH_2O$. It is worth mentioning that the capacity retention is increased at high current density. This is the common phenomenon for LiV_3O_8 cathode materials [12,33,34]. It is believed that more available sites for Li ions could be used at low current density, some of which probably possess the inferior reversibility of Li^+ insertion and extraction.

To further understand the good cycling stability of $Na_2V_6O_{16}{\cdot}0.86H_2O$ electrode, Nyquist plots at 2.5 V after different cycles (3rd and 80th in Fig. 9) at 150 mA g^{-1} are given in Fig. 10. As shown, each impedance spectrum consists of a depressed semicircle at the high frequency followed by a slope line at the low frequency range. The depressed semicircle is attributed to charge-transfer impedance, while the slope line is due to Warburg impedance which reflects lithium ion diffusion in the solid state

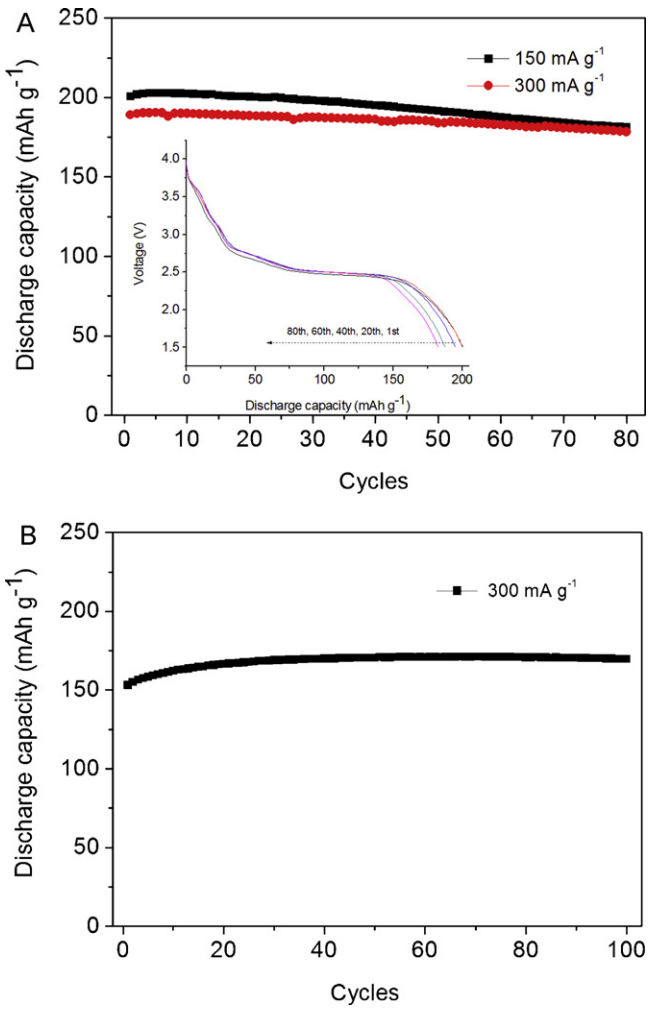

Fig. 9. Long cycling performance of annealed $Na_2V_6O_{16}{\cdot}xH_2O$ electrodes: (a) with thermal treatment at 300 °C at 150 and 300 mA g^{-1}, respectively, together with the different discharge curves at 150 mA g^{-1} (1st, 20th, 40th, 60th, and 80th) inset and (b) with thermal treatment at 400 °C at 300 mA g^{-1}.

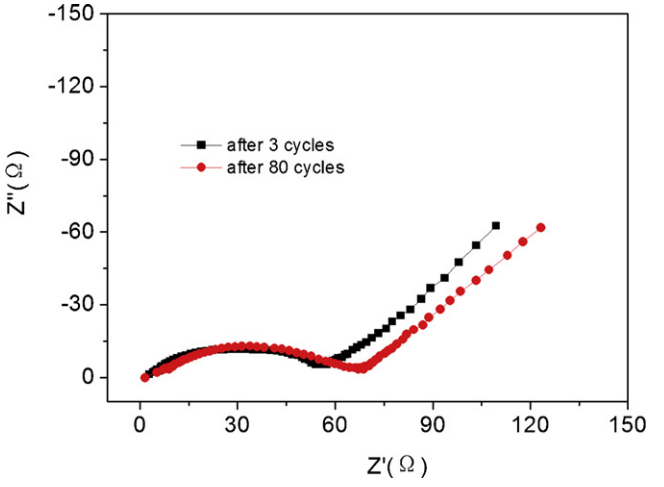

Fig. 10. Nyquist plots of the $Na_2V_6O_{16}{\cdot}0.86H_2O$ electrode at 2.5 V after 3 and 80 cycles at 150 mA g^{-1}.

electrodes [35,36]. For comparison, no considerable difference in both impedance spectra of $Na_2V_6O_{16}\cdot 0.86H_2O$ electrode is discovered, implying the charge-transfer impedance keeps stable during the long cycling test, which is consistent with the cycling performance in Fig. 9.

4. Conclusions

In summary, a new cathode material, $Na_2V_6O_{16}\cdot 2.36H_2O$ nanowire with diameter of 60–100 nm and length of up to 5 μm was synthesized for lithium ion battery by a facile hydrothermal reaction. It presented an initial discharge capacity of 268 mAh g^{-1} but poor cycling stability. It was found that appropriate thermal treatment could remove part of crystal water and shrink the crystal, resulting in much improved cycling stability. Moreover, higher heating temperature meant much better cycling stability, but decreasing capacity. $Na_2V_6O_{16}\cdot 0.86H_2O$ treated at 300 °C showed an initial discharge capacity of 235 mAh g^{-1} at 30 mA g^{-1} with the discharge capacity of 214.7 mAh g^{-1} maintaining after 30 cycles. Capacity retention of 90.4% and 94.4% was achieved at 150 and 300 mA g^{-1}, respectively, after 80 cycles. Annealed $Na_2V_6O_{16}\cdot xH_2O$ here could be proposed as a potential cathode material for Li-ion battery.

Acknowledgements

Financial support from the Major State Basic Research Development Program of China (973 Program) (No. 2010CB227204), the National Natural Science Foundation of China (No. 50972165), Research Funding of Hunan Province for Ph.D. Student (No. CX2010B114), Graduate Degree Thesis Innovation Foundation of Central South University is greatly appreciated. H. Wang thanks to financial support from the Chinese Government Scholarship.

References

[1] J.M. Tarascon, M. Armand, Nature 414 (2001) 359–367.
[2] Y.K. Sun, J.M. Han, S.T. Myung, S.W. Lee, K. Amine, Electrochem. Commun. 8 (2006) 821–826.
[3] M.S. Whittingham, Chem. Rev. 104 (2004) 4271–4301.
[4] A.R. Armstrong, A.J. Paterson, A.D. Robertson, P.G. Bruce, Chem. Mater. 14 (2002) 710–719.
[5] M. Winter, J.O. Besenhard, M.E. Spahr, P. Novák, Adv. Mater. 10 (1998) 725–763.
[6] A.D. Tang, H.Y. Wang, K.L. Huang, B. Tan, X.L. Wang, Prog. Chem. 19 (2007) 1313–1321.
[7] T. Ohzuku, Y. Makimura, Chem. Lett. 30 (2001) 642–643.
[8] N.A. Chernova, M. Roppolo, A.C. Dillon, M.S. Whittingham, J. Mater. Chem. 19 (2009) 2526–2552.
[9] J. Jiang, Z.X. Wang, L.Q. Chen, J. Phys. Chem. C 111 (2007) 10707–10711.
[10] H.M. Liu, Y.G. Wang, L. Li, K.X. Wang, E. Hosono, H.S. Zhou, J. Mater. Chem. 19 (2009) 7885–7891.
[11] S. Panero, M. Pasquali, G. Pistoia, J. Electrochem. Soc. 130 (1983) 1225–1227.
[12] H.M. Liu, Y.G. Wang, K.X. Wang, Y.R. Wang, H.S. Zhou, J. Power Sources 192 (2009) 668–673.
[13] G.Q. Liu, C.L. Zeng, K. Yang, Electrochim. Acta 47 (2002) 3239–3243.
[14] H.Y. Wang, K.L. Huang, S.Q. Liu, C.H. Huang, W.J. Wang, Y. Ren, J. Power Sources 196 (2011) 788–792.
[15] J. Kawakita, T. Miura, T. Kishi, Solid State Ionics 124 (1999) 21–28.
[16] J. Kawakita, T. Miura, T. Kishi, Solid State Ionics 124 (1999) 29–35.
[17] M.E. Spahr, P. Novák, W. Scheifele, O. Haas, R. Nesper, J. Electrochem. Soc. 145 (1998) 421–427.
[18] G.T. Zhou, X.C. Wang, J.C. Yu, Cryst. Growth Des. 5 (2005) 969–974.
[19] J.G. Yu, J.C. Yu, W.K. Ho, L. Wu, X.C. Wang, J. Am. Chem. Soc. 126 (2004) 3422–3423.
[20] W.A. Jr., C. Ribeiro, E.R. Leite, V.R. Mastelaro, Mater. Chem. Phys. 127 (2011) 56–61.
[21] E.M. Sipple, P. Bracconi, P. Dufour, J.C. Mutin, Solid State Ionics 141–142 (2001) 455–461.
[22] B. Azambre, M.J. Hudson, O. Heintz, J. Mater. Chem. 13 (2003) 385–389.
[23] L.Q. Mai, C.S. Lao, B. Hu, J. Zhou, Y.Y. Qi, W. Chen, E.D. Gu, Z.L. Wang, J. Phys. Chem. B 110 (2006) 18138–18141.
[24] N. Li, C.R. Martin, B. Scrosati, J. Power Sources 97–98 (2001) 240–243.
[25] P.G. Bruce, B. Scrosati, J.M. Tarascon, Angew. Chem. Int. Ed. 47 (2008) 2930–2946.
[26] C.H. Jiang, E. Hosono, H.S. Zhou, Nanotoday 1 (4) (2006) 28–33.
[27] J. Kawakita, M. Majima, T. Miura, T. Kishi, J. Power Sources 66 (1997) 135–139.
[28] A.D. Wadsley, Acta Crystallogr. 10 (1957) 261–267.
[29] K. West, B. Zachau-Christiansen, S. Skaarup, Y. Saidi, J. Barker, I.I. Olsen, R. Pynenburg, R. Koksbang, J. Electrochem. Soc. 143 (3) (1996) 820–825.
[30] H.Y. Wang, K.L. Huang, S.Q. Liu, Y. Luo, Chin. J. Inorg. Chem. 25 (2009) 2090–2096.
[31] D.C. Li, Y. Sasaki, K. Kobayakawa, Y.C. Sato, Electrochim. Acta 51 (2006) 3809–3813.
[32] H.Y. Wang, K.L. Huang, C.H. Huang, S.Q. Liu, Y. Ren, X.B. Huang, J. Power Sources 196 (2011) 5645–5650.
[33] A.Q. Pan, J. Liu, J.G. Zhang, G.Z. Cao, W. Xu, Z.M. Nie, X. Jie, D. Choi, B.W. Arey, C.M. Wang, S.Q. Liang, J. Mater. Chem. 21 (2011) 1153–1161.
[34] F.H. Tian, L. Liu, Z.H. Yang, X.Y. Wang, Q.Q. Chen, X.Y. Wang, Mater. Chem. Phys. 127 (2011) 151–155.
[35] Y.J. Kang, J.H. Kim, S.W. Lee, Y.K. Sun, Electrochim. Acta 50 (2005) 4784–4791.
[36] F. Nobili, F. Croce, B. Scrosati, R. Marassi, Chem. Mater. 13 (2001) 1642–1646.